

# Gold Nanoparticle Uptake and Mechanism Elucidation

Contact [f.j.currell@qub.ac.uk](mailto:f.j.currell@qub.ac.uk)

Fred Currell, Laura Taggart, Harold McQuaid, Chris Polin, Kevin Prise, James Nichol, Jonathan Coulter  
Queen's University, Belfast, UK

Stan Botchway  
STFC, Rutherford Appleton Laboratory, UK

Dorian Dixon  
University of Ulster, UK

## Introduction

Gold nanoparticles (AuNPs) are ubiquitous in the field of nanomedicine. About 50% of all publications concerning the medical applications of nanoparticles concern those with a gold core. Considered to be both biocompatible and chemically versatile, AuNPs afford functionalization routes through the addition of biologically active groups that confer specific biological function(s) to the nanoparticles. Use of AuNPs across a range of applications has been covered in a Nature special edition [1] while their use in cancer therapeutics is outlined in [2].

It is of interest to learn how parameters like the surface coating, nanoparticle size and nanoparticle morphology affect the cellular uptake. Clearly then, techniques to image such nanoparticles efficiently within cells are important and need development. Fluro-tagging the nanoparticle and then inferring the subcellular distribution from the corresponding fluorescence signal is one means commonly used to this end. However detachment of the fluro-tag can AuNPs are observed to form clusters inside various cell compartments [3]. In such cases the resultant image does not report the gold distribution but instead only reports the fluorescent group's distribution.

In comparison, the approach we are investigating images the gold core directly - the nanoparticle's surface plasmon resonance is used instead providing an intrinsic detection method. Furthermore since the peak wavelength of the plasmon resonance depends on the nanoparticle size [4] it is possible to make inferences about the degree of clumping taking place.

## Method

For mechanistic studies into the relationship between gold uptake and mitochondrial function cells were seeded onto 4-Chamber Slides (Sigma Aldrich) and left to attach for 4-6 hours before treatment. Once incubated with GNPs for various times the cells were treated with 10 nM MitoTracker Red CMXRos (Invitrogen) in cell media for 30 mins prior to fixing with paraformaldehyde solution for 10 mins. In other studies aimed at comparing uptake of different nanoparticles a similar procedure was used although MitoTracker was not used.

In MPR microscopy, a short pulsed (~200 fs), tightly focused laser beam (typ.  $\lambda = 600$  nm) excites the localised surface plasmon resonance of the gold nanoparticles [5]. The decay of the plasmon resonance results in UV photons, which after passing through a UV band pass filter were detected using a photomultiplier tube. The lifetime of the decay was measured and time-correlated with the time information being used to separate the non-linear excitation of gold nanoparticles (fast component) from that of the cytoplasm or nuclear DNA (slow component).

The UV photons were detected after passing through a UV band pass (U340, Comar UK) filter and focused using a Hamamatsu

R3809-U photomultiplier tube. The characteristic lifetime of the decay was measured using a Becker and Hickl time-correlated single-photon counting system (SPC830) and software (SPCImage version 3.7). This process was repeated many times as the laser was raster-scanned across the sample with the fluorescence lifetime decay collected for each separate x,y location. For each location the lifetime decay was analysed in terms of a fast and slow component. Images were created showing the amount of fast-component present in each pixel and these images were co-registered with conventional confocal images that showed the immunofluorescent stain uptake. Such images provide a means to correlate AuNP uptake with cell structure and/or function, depending on the stains used.

Live cell imaging is also possible with this set up. To achieve this, the fixed cells were replaced with live cells held in dish with both thermal and atmosphere control. This was done with alternate confocal and MPR microscopy images being taken every few minutes for several hours.

## Results

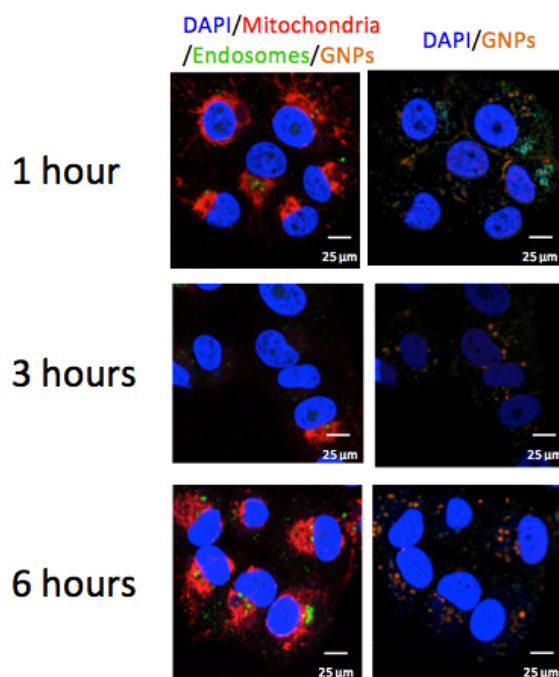


**Fig.1** Colocalised MPR and confocal images of MDA-MB-231 cells were treated with GNPs for various times (indicated), MitoTracker (red) shows mitochondrial membrane polarization, (green) shows an early endosomal antibody, while DAPI shows the nuclei (blue) and GNPs are shown in (orange). In the second column the same images are shown but with only the (blue) and (orange) channels showing to make it easier to discern the gold.

Figure 1 shows examples of the results taken to look at the correlation between mitochondrial activity and gold uptake. Many similar images have been measured for three cells lines and taken together and supported by other measurements made in our own laboratory they support the conclusion that a key players in the mechanism is radiosensitisation of cells by GNPs are oxidative stress and the mitochondria [6].

Figure 2 shows how the uptake of GNPs with Citrate, PEG and PEG-RME coatings. The Citrate coating is commonly used in the synthesis of GNPs. Whilst citrate coating leads to good cellular uptake, it is not considered suitable for *in vivo* work, where Polyethylene Glycol (PEG) coatings are more commonly used. As is shown in figure 2, the PEG coating acts to compromise the cellular uptake. However this uptake can be rescued using targeting peptides such as RME. This study shows the benefit of MPR-microscopy for developing new GNP formulations as it provides a rapid assessment of their uptake.

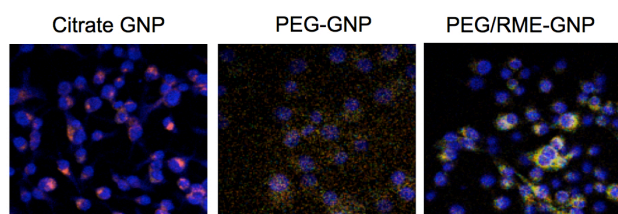


**Fig.2** MPR and confocal images of MDA-MB-231 cells were treated with GNPs with various coatings (indicated) for 6 hours prior to fixing. DAPI shows the nuclei (blue) and GNPs density is shown in a heat-map (low density: green to high density orange).

In a third experiment we performed live-cell imaging from 10 minutes after addition of the GNPs to learn more about the uptake dynamics. Alternately single MPR and confocal images were taken every few minutes. Although we were successful in seeing the gold and its very rapid uptake, we were unable to track discernable features across significant periods. The laser used for the MPR microscopy has a tight waist that only extends for a short distance along the beam (z) direction. This means that the gold is only detected in a narrow slice, perhaps only 500 nm thick. A cluster of GNPs moving with a velocity component perpendicular to this slice will only appear in one or two frames as they pass through this plane. Whilst the frames we acquired provide proof of principle for the live-cell imaging capability of MPR microscopy, we believe that new data acquisition modes will allow us to use this technique to properly track uptake dynamics.

### Ongoing/Future developments

Clearly MPR microscopy is proving a valuable tool in both elucidating mechanism of GNP action on cells and in developing suitable bio-functionalised coatings able to facilitate high intracellular uptake. We hope to extend these studies in the near future, considering the effect on uptake of factors such as PEG linker length and amount of coating agent per nanoparticle.

We also expect the live-cell imaging to be a valuable asset in learning about mechanism of uptake, provided we can overcome the issue that the nanoparticles are only visible in the thin horizontal slice. To this end we will implement two new data acquisition methods. Firstly, we will asynchronously scan the Z-position of the microscope, thereby integrating over a wider range of Z (effectively making the PSF in that direction several microns). The resultant MPR image will thus be a projection of this range of Z-positions, allowing for tracking of the nanoparticles in 2-D. More ambitiously, we will implement Becker and Hickl's FIFO imaging mode [<http://www.becker-hickl.com/pdf/fifo-imaging05.pdf>] whereby for each photon

detected a full record is created, including the x-y-z position of the laser focus in the sample and detection time relative to the laser pulse. This data-recording technique (commonly known as 'list mode' in particle physics) allows one to perform off-line reconstruction of the data, performing projections and cuts of interest. Collecting data in this way whilst scanning the laser focus position in x-y (galvanometers) and z (microscope objective position) will then allow us to reconstruct 3-D data sets showing the dynamics of the GNPs in living cells. As well as significantly advancing our own project, we expect this new acquisition mode will be of significant benefit to other users of the facility.

### Conclusions

MPR is a powerful approach to imaging gold nanoparticles and the clusters the form in fixed cells. The ability to co-register multiphoton (gold location) images with traditional confocal images is useful for both mechanistic and uptake studies. Future developments should allow these benefits to be extended to shorter times and with more comprehensive dynamical information through the implementation of new data acquisition modes to be used alongside live-cell imaging.

### Acknowledgements

We wish to thank the members of the Queen's University gold nanoparticle dose enhancement group and the staff of the Research Complex at Harwell who have made this research possible. We also thank the Department of Learning Northern Ireland, Cancer Research UK and the Science and Technologies Facility Council for financial support, which has underpinned this research.

### References

1. Brody H (ed). Gold. Nature Supplement 2013;495:S1-S45
2. Conde J et al, Journ. Drug Deliv, 2012 Article ID 751075
3. J A Coulter et al, "Cell type-dependent uptake, localization, and cytotoxicity of 1.9 nm gold nanoparticles" Intl. J. Nanomed 7, 2673-2685 (2012)
4. P. N. Njoki et al, "Size Correlation of Optical and Spectroscopic Properties for Gold Nanoparticles" J. Phys. Chem. C 111 14664-14669, (2007)
5. D. Yelin et al, "Multiphoton plasmon-resonance microscopy" Optic Express, 2003;11: 1385-1391
6. L. Taggart et al, "Gold nanoparticles: radioenhancer or radiosensitiser?" *in prep* (2013)

# The use of FLIM to measure the stabilities of metal complexes in living cells

Contact Stan.Botchway@stfc.ac.uk

J.R. Dilworth, S. Faulkner, M.W. Jones, M.B.M. Theobald and P.A. Waghorn

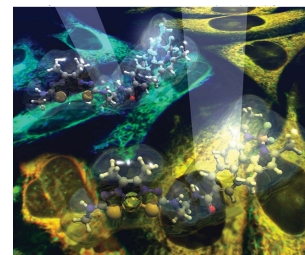
University of Oxford  
Inorganic Chemistry Department, South Parks Road, Oxford

S. Pascu and R.Arrowsmith

University of Bath  
Chemistry Department, Bath, BA2 7AY

S. Botchway and A. Parker

Central Laser Facility  
Rutherford Appleton Laboratory,  
Harwell Science and Innovation  
Campus, Oxon OX11 0QX



## Introduction

Metal complexes are widely used in medicine for both imaging and therapy. Many of these depend on intracellular processes to achieve selectivity but since the majority of analytical methods focus on the metal, little is known about the speciation of such species in living cells. The resolution limit for nuclear medicine of 1-2mm means that it is not applicable at the cellular level. Confocal fluorescence microscopy has been used extensively to track compounds and follow processes in cells and we have designed a series of fluorescent metal complexes which can be followed in cells by virtue of their 1 or 2-photon fluorescence. While the emission wavelength of a ligand may not change when a metal is coordinated the emission lifetime does and this provides a potential method to determine when and where dissociation of a metal complex occurs within a cell. We have explored the use of this approach to determine if and when intracellular demetallation of biologically active metal complexes occurs. The work described here has recently been published (ChemSci, 2013, 4, 1430-1441) with the cover picture shown at the top right of this page.

## Copper, nickel and zinc bis(thiosemicarbazone) complexes

The studies described here are focussed on bis(thiosemicarbazone) complexes as copper(II) complexes such as CuATSM are in current clinical use for the imaging of hypoxia<sup>1,2</sup> and have been investigated for the treatment of Alzheimer's disease.<sup>3</sup> The hypoxic selectivity is proposed to depend on the reduction of the complexes in hypoxic cells followed by dissociation of the copper and subsequent cellular metabolic trapping.<sup>4</sup> It has been proposed that the analogue without methyl groups on the backbone (CuGTS) under aerobic conditions liberates copper which inhibits formation of amyloid aggregates. However nothing is known about the dissociative mechanism in living cells for this class of complex and as the simple complexes are not fluorescent we have attached fluorophores to the CuATSM core in order to follow the fate of the complexes in cells. The structures of the complexes used in this study are shown in Figure 1.

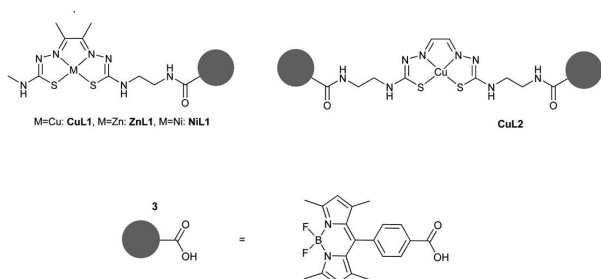


Figure 1: Structures of bodipy appended ligands and complexes used in this study

Following detailed studies in solution the behaviour of the complexes and ligands in living cells was followed using 2-photon fluorescence and FLIM measurements. We elected to use two photon excitation to minimize autofluorescence within the cells and the data obtained was of significantly higher quality than with single photon excitation. Solutions at concentrations of 10 $\mu$ M were added to suspensions of HeLa cells in glass bottomed Petri dishes in serum free EMEM medium and fluorescence studies carried out after ca. 20 minutes of incubation in air.

Figure 2 shows the fluorescence lifetime maps and sample point decay curves for L1, CuL1 and NiL1.

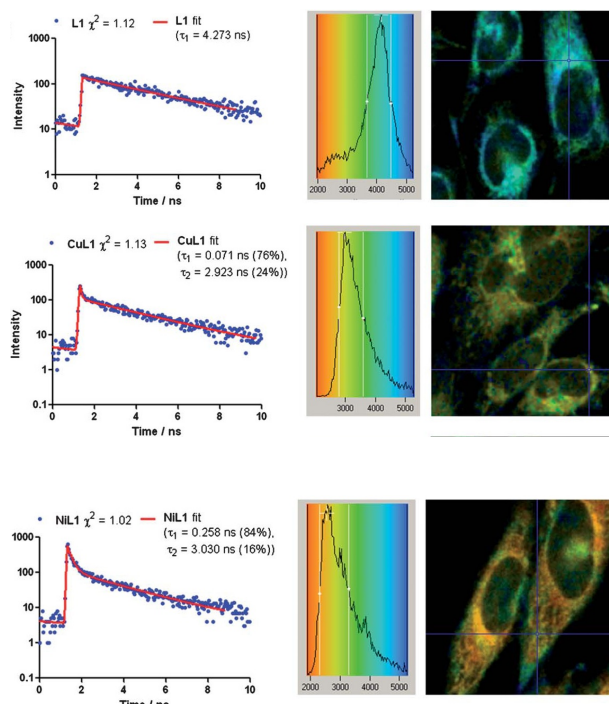
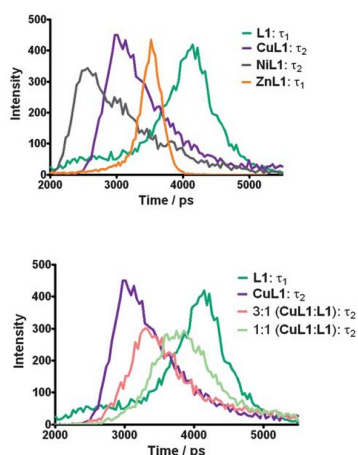


Figure 2: Sample point decay curves and lifetime cell maps for ligand L1 and its complexes with copper and nickel. The colours in the cell map are representative of the lifetime distributions at each point in the cell.

The point decay curves for the free ligand could be fitted to a single decay process whereas there were two distinct processes for the Cu and Ni complexes. The short lifetime process was associated with a metal being present and suggested that under aerobic conditions the complexes remain essentially intact inside the cells. The global lifetime distributions (GLD) within the cells are summarized in Figure 3 (top) and show that the

lifetime distributions are quite distinct for the free ligand and the complexes



**Figure 3:** Overlays of global lifetime distributions for L1, CuL1, NiL1 and ZnL1 (top) and showing the effect on GLDs of the addition of various ratios of CuL1 to ligand to cells (lower).

To confirm that it was indeed possible to detect the free ligand in the presence of intact complexes we investigated the lifetime maps in HeLa cells for free ligand L1 and various ratios of CuL1 to L1. The presence of free ligand causes a shift of the GLD from that of the complex towards the value for the ligand alone (see Figure 3). There was also little or no loss of fluorescence intensity or change in the GLD for CuL1 after the treated cells were allowed to stand for two hours, suggesting the complex was stable over this time scale. The analysis of the data for the ZnL1 complex was less straightforward as intact metal complex even in solution did not show the short lifetime decay of the Cu and Ni complexes perhaps due to the closed shell  $d^{10}$  configuration of Zn(II).

The behaviour of the Cu(II) complex of ligand L2 was entirely different. The point decay curves and the lifetime maps of the ligand and Cu complex in HeLa cells were recorded as before and are shown in Figure 4a and 4b.

2

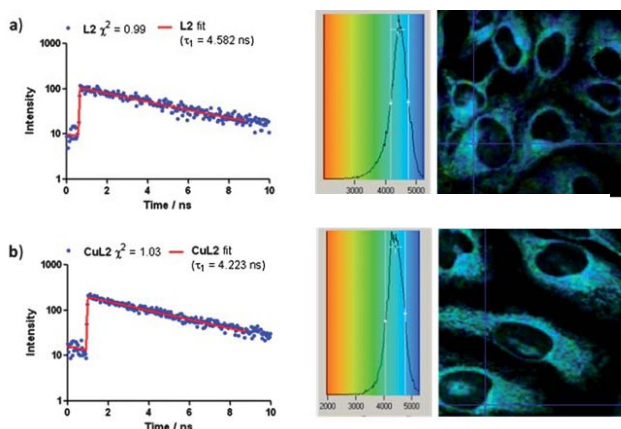


**Figure 4:** Point decay curves and lifetime maps for L2 and CuL2 in HeLa cells.

The point decay curve shows no evidence for the short lifetime decay characteristic of the presence of the Cu(II), as was seen in the solution measurements, and the lifetime maps, GLD and decay curves appear virtually identical for complex and ligand. We conclude that the Cu complex of L2 is completely dissociated in cells.

## Conclusions

We have demonstrated that 2-photon FLIM measurements can be used to show for the first time that complexes of the type CuL1 remain largely undissociated in HeLa cells under aerobic conditions. This complements the data obtained under aerobic and hypoxic conditions for 64-Cu radiolabelled CuATSM and has contributed to a major revision of the mechanism of hypoxic selectivity.<sup>5</sup> There is a dramatic change in cellular stability of the bis(thiosemicarbazonato)Cu complexes when there are no methyl groups on the ligand backbone and the complex CuL2 is completely dissociated. This provides definitive evidence to support the proposal based on solution measurements that these complexes liberate copper ions in cells and thereby act as inhibitors of amyloid protein aggregates.

This study focused on thiosemicarbazones as there were specific questions about their mechanisms of biological action that could be addressed. However we have preliminary evidence to suggest that this technique is also applicable to range of other metal complexes. The use of near IR emitting fluorophores also offers the possibility of determining metal complex stability in whole blood and we plan to continue to investigate the scope of this approach in biology and medicine in the future.

## Acknowledgements

We thank the EPSRC (PAW, RLA), Siemens Molecular Imaging (MBMT) and MRC (MWJ, SIP) for financial support, the Royal Society for a University Research Fellowship (SIP) and STFC and RCaH, Harwell Oxford for a programme grant and support. We thank Dr Pierre Burgos, Dr Rahul Yadav, Dr Selene Roberts, Mr Alistair Mackenzie and Mr Alex Henman for assistance with cell biology and fluorescence lifetime measurements at RAL.

## References

1. Dehdashti, F. *et al.* In vivo assessment of tumor hypoxia in lung cancer with Cu-60-ATSM. *European Journal of Nuclear Medicine and Molecular Imaging* **30**, (2003).
2. Vavere, A. L. & Lewis, J. S. Cu-ATSM: A radiopharmaceutical for the PET imaging of hypoxia. *Dalton Trans.*, 4893-4902 (2007).
3. Donnelly, P. S. *et al.* Selective Intracellular Release of Copper and Zinc Ions from Bis(thiosemicarbazonato) Complexes Reduces Levels of Alzheimer Disease Amyloid- $\beta$  Peptide. *J. Biol. Chem.* **283**, 4568-4577, (2008).
4. Obata, A. *et al.* Retention mechanism of hypoxia selective nuclear imaging/radiotherapeutic agent Cu-diacetyl-bis(N4-methylthiosemicarbazone) (Cu-ATSM) in tumor cells. *Ann. Nucl. Med.* **15**, 499-504 (2001).
5. R. Hueting, V. Kersemans, B. Cornelissen, M. Tredwell, K. Hussien, M. Christlieb, A D Gee, J. Passchier, S C Smart, J R Dilworth, V. Gouverneur and R J Muschel *J. Nucl. Med.*, 2013, *accepted for publication*

# The plant secretoryome Part II: Golgi stack N-glycosylation enzymes interaction studies using Fluorescence Lifetime Imaging Microscopy

Contact [chawes@brookes.ac.uk](mailto:chawes@brookes.ac.uk) and [jennifer.schoberer@boku.ac.at](mailto:jennifer.schoberer@boku.ac.at)

Jennifer Schoberer<sup>1,2</sup>, Eva Liebminger<sup>1</sup>, Stanley W. Botchway<sup>3</sup>, Richard Strasser<sup>1</sup>, Chris Hawes<sup>2</sup>

<sup>1</sup> Department of Applied Genetics and Cell Biology, University of Natural Resources and Life Sciences, BOKU Vienna, Muthgasse 18, 1190 Wien, Austria

<sup>2</sup> Department of Biological and Medical Sciences, Faculty of Health and Life Sciences, Oxford Brookes University, Gypsy Lane, Headington, Oxford OX3 0BP, United Kingdom

<sup>3</sup> Central Laser Facility, STFC, Rutherford Appleton Laboratory, Harwell Science & Innovation Campus, Didcot, OX11 0QX, United Kingdom

## Introduction

The plant cell Golgi apparatus is a key organelle that modifies, sorts, and packages proteins. Its structure and mobility are thought to determine its function. Protein and lipid modifications, sorting of molecules as well as the biosynthesis of cell wall polysaccharides, all take place in the small stacks of flattened cisternae that make up the Golgi apparatus in plant cells. Among the various post-translational modification reactions on proteins, the biosynthesis and processing of protein-bound N-linked oligosaccharides (N-glycans) is the most common. N-glycans play a crucial role in protein folding, endoplasmic reticulum quality control (Liu and Howell, 2010), biotic (Saijo, 2010), and abiotic stress response (Koiwa et al., 2003; Kang et al., 2008) and are considered essential for the physico-chemical properties and biological functions of glycoproteins. All Golgi-resident plant N-glycan processing enzymes are so-called type II membrane proteins with an N-terminal region comprising a short cytoplasmic tail (C), a single transmembrane domain (T), and a luminal stem region (S), together called the CTS region, which orients the C-terminal catalytic domain (CD) into the Golgi lumen. To date it is not known which signals or mechanisms define their strict intra-Golgi location. One suggested mechanism is the formation of enzyme complexes which leads to their retention in the Golgi membranes. There is evidence for the formation of glycosyltransferase complexes involved in various aspects of plant cell wall biosynthesis, but it is uncertain whether enzymes involved in N-glycan processing assemble into similar complexes. To address this question, we have tested the properties of several glycosidases and glycosyltransferases with distinct intra-Golgi locations to form protein-protein interactions when expressed transiently in tobacco (*Nicotiana* spp.) leaves.

In this report we describe the use of two-photon (2P)-excitation Förster resonance energy transfer (FRET)-fluorescence lifetime imaging microscopy (FLIM) to determine the interaction of N-glycan processing enzymes with differential intra-Golgi locations.

**Two *cis*/medial-Golgi enzymes MNS1 and GnTI form *in vitro* and *in vivo* interactions:** Using the two *cis*/medial-Golgi residents MNS1 (*Arabidopsis thaliana* Golgi  $\alpha$ -mannosidase I, Liebminger et al., 2009) and GnTI (*Nicotiana tabacum*  $\beta$ 1,2-N-acetylglucosaminyltransferase I, Schoberer et al., 2009) as putative candidate proteins we tested whether plant N-glycan processing enzymes are able to form glycosyltransferase

complexes using GFP and mRFP fused to full-length clones of MNS1, designated as MNS1-G (G standing for GFP) and MNS1-R (R standing for mRFP), and GnTI, designated as GnTI-G and GnTI-R. Both enzymes are known to be involved in the processing of oligomannosidic to hybrid N-glycans and hence act early in the N-glycan processing pathway. These fusion proteins were transiently expressed in tobacco leaves under the control of the 35S promoter.

**Table 1.** Fluorescence lifetimes of full-length *cis*- and medial-Golgi enzyme pairs

donor	acceptor	$\tau \pm$ SD (ns)	$\tau$ range	<i>n</i>
MNS1-G		$2.2 \pm 0.1$	1.8-2.4	343
MNS1-G	MNS1-R	$1.9 \pm 0.1$	1.7-2.2	195
GnTI-G		$2.2 \pm 0.1$	1.9-2.4	283
GnTI-G	MNS1-R	$1.9 \pm 0.1$	1.6-2.2	342
GnTI-G		$2.2 \pm 0.1$	1.9-2.4	283
GnTI-G	GnTI-R	$1.9 \pm 0.1$	1.6-2.1	275

**Abbreviations:**  $\tau$ , average GFP lifetime; SD, standard deviation; range  $\tau$ , range of lifetimes observed for the respective sample; *n*, number of analysed Golgi stacks.

## Subcellular location of MNS1 and GnTI

Expression levels and efficient targeting of the fusion proteins to the Golgi were confirmed by live-cell confocal imaging. Merged confocal images show considerable colocalisation of co-expressed protein pairs MNS1-G/MNS1-R (Figure 1A-C), GnTI-G/GnTI-R (Figure 1D-F), and GnTI-G/MNS1-R (Figure 1G-I) in Golgi bodies of tobacco leaf epidermal cells.

Confocal images of representative tobacco leaf epidermal cells co-expressing fluorescent-protein tagged full-length protein pairs MNS1-G (A) and MNS1-R (B), GnTI-G (D) and GnTI-R (E), and GnTI-G (G) and MNS1-R (H). Images C, F, and I show a merge of green (GFP fluorescence) and magenta (mRFP fluorescence) channels. White in merged images indicates areas of co-localisation. Abbreviations: G, GFP; R, mRFP. Scale = 5  $\mu$ m.

### In vivo 2-photon-FRET-FLIM

To determine whether the interactions previously found by co-immunoprecipitation (co-IP) also occur in live plant cells, we used 2P-FRET-FLIM to confirm the interaction. Tobacco leaf cells expressing MNS1-G or GnTI-G alone were used as controls to establish the unquenched lifetime of GFP in the context of the fusion proteins (serving as donors). Figure 2

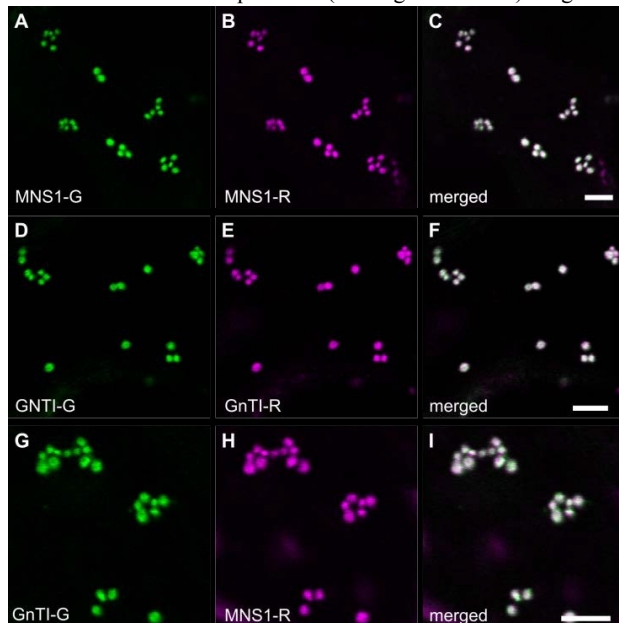


Figure 1. Golgi localisation of full-length *cis*/medial-Golgi protein pairs in tobacco leaves.

shows representative confocal and pseudo-coloured lifetime images of a control cell expressing the donor MNS1-G alone (Figure 2B-D) or a cell expressing the donor in the presence of

the acceptor MNS1-R (Figure 2E-G). We determined an average excited-state fluorescence lifetime of  $2.2 \pm 0.1$  nanoseconds (ns) for MNS1-G (Figure 2D) following FLIM measurements in the absence of an acceptor. Co-expression of MNS1-G and MNS1-R led to a significant quenching of the donor lifetime to an average of  $1.9 \pm 0.1$  ns (Figure 2G), which

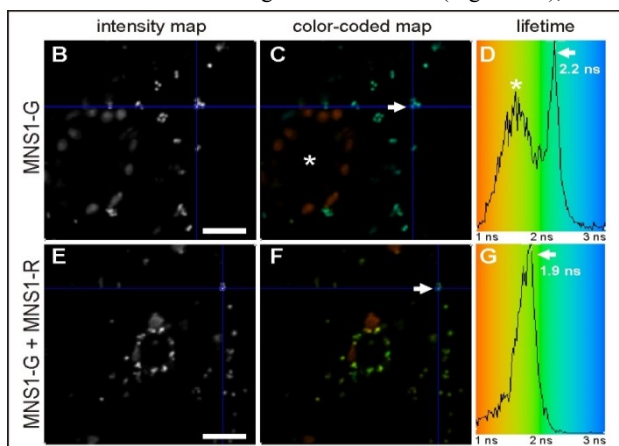


Figure 2: B-D control cell showing expression of a donor fusion protein MNS1-G. E-G self-interaction of MNS1-G with MNS1-R showing reduced lifetime of (1.9 compared with 2.2 for B-D).

indicates that the fluorophores of the analysed protein pair were close enough in Golgi membranes to undergo FRET and that MNS1-G likely interacts with MNS1-R. For GnTI-G, the average fluorescence lifetime was  $2.2 \pm 0.1$  ns in the absence of the acceptor, but decreased to an average of  $1.9 \pm 0.1$  ns in the presence of GnTI-R or MNS1-R (data not shown), indicating interactions between GnTI-G/GnTI-R and GnTI-G/MNS1-R.

Altogether, the established FRET-FLIM data are consistent with the co-IP data and we can conclude that at least the two tested N-glycan processing enzymes MNS1 and GnTI homodimerise and additionally form a GnTI/MNS1 heterodimer. It is worth noting that the excited-state lifetime of GFP-tagged proteins alone in live cells (plants and animal) is around 2.5 ns. Here this is further reduced due to self-quenching by possible homodimerisation.

### Conclusion

Using the non-invasive 2P-FRET-FLIM biophysical method, we have observed the formation of several homo- and heterodimers between *cis*- and medial-Golgi enzymes, namely MNS1, GnTI, GMII and XylT, whereas only one heterodimer between GALT1 and GMII was observed among the late-acting enzymes GALT1, FUT13 and ST (a non-plant Golgi marker).

### Acknowledgements

Christiane Veit and Alexandra Castilho (BOKU Vienna) as well as Janet Evins and Anne Kearns (Oxford Brookes) are thanked for their excellent technical assistance. This project was funded by an Erwin-Schrödinger fellowship from the Austrian Science Fund (FWF) project J2981-B20 (to J.S.), FWF project P23906-B20 (to R.S.), and Oxford Brookes University. This work is now published in Plant Physiology 2013 (reference 6, Copyright American Society of Plant Biologists).

### References

1. Liu JX, Howell SH (2010) Endoplasmic reticulum protein quality control and its relationship to environmental stress responses in plants. *Plant Cell* 22: 2930-2942
2. Saijo Y (2010) ER quality control of immune receptors and regulators in plants. *Cell Microbiol* 12: 716-724.
3. Saijo Y (2010) ER quality control of immune receptors and regulators in plants. *Cell Microbiol* 12: 716-724
4. Liebming E, Hüttner S, Vavra U, Fischl R, Schoberer J, Grass J, Blaukopf C, Seifert GJ, Altmann F, Mach L, Strasser R (2009) Class I alpha-mannosidases are required for N-glycan processing and root development in *Arabidopsis thaliana*. *Plant Cell* 21: 3850-3867
5. Schoberer J, Vavra U, Stadlmann J, Hawes C, Mach L, Steinkellner H, Strasser R (2009) Arginine/lysine residues in the cytoplasmic tail promote ER export of plant glycosylation enzymes. *Traffic* 10: 101-115
- Schoberer J, Liebming E, Botchway SW, Strasser R, Hawes C. (2013) Time-resolved fluorescence imaging reveals differential interactions of N-glycan processing enzymes across the Golgi stack in planta. *Plant Physiol.* 161:1737-1754.

## Characterisation of small fluorescent protein iLOV for use in fluorescence lifetime imaging applications

**Contact** [sarahirons@brookes.ac.uk](mailto:sarahirons@brookes.ac.uk)

**Sarah L. Irons**

*Oxford Brookes University, Department of Biological and Medical Sciences. Headington, Oxford, UK*

**Leo Graves**

*Oxford Brookes University, Department of Biological and Medical Sciences. Headington, Oxford, UK*

**L. A. King**

*Oxford Brookes University, Department of Biological and Medical Sciences. Headington, Oxford, UK*

**Stan W. Botchway**

*STFC, Rutherford Appleton Laboratory. Chilton, Didcot, UK.*

The author has requested that this article is not included on the web.



# Ultrasensitive Dark-Field Microspectroscopy with a Super Continuum Source

Contact [philipp.kukura@chem.ox.ac.uk](mailto:philipp.kukura@chem.ox.ac.uk)

A Weigel, A Sebesta, P Kukura

*Physical and Theoretical Chemistry*

*University of Oxford*

*South Parks Road*

*Oxford OX1 3QZ*

## Introduction

The advent of single particle optics has had a profound impact on a large variety of fields ranging from genetics all the way to quantum optics.<sup>1</sup> For truly nanoscopic particles and single emitters all current detection techniques rely exclusively on the efficient detection of fluorescence. Therefore, fundamental questions, such as the fate a quantum dot or a fluorophore, when it ceases to emit light (blinking or bleaching), still remain unsolved. Extinction of light, on the other hand, is largely independent of excited state relaxation and can detect particles even in their 'dark' state. The long-held notion that detection of the absorption of a single molecule is impossible was recently disproved.<sup>2-4</sup> Extending such experiments from mere detection to broadband spectroscopy will provide a completely new view on single particle properties beyond the limitations of fluorescence spectroscopy.

Dark-field scattering microscopy directly detects the photons, which are elastically scattered by a particle away from the excitation beam. As fluorescence, the technique is in principle background-free, and therefore provides the ideal starting point for the development of an ultra-sensitive extinction spectrometer. Here, we have developed a detection geometry for dark field microspectroscopy that allows us to collect white light scattered from a particle with 95% of the numerical aperture of the objective. Losses in the detection arm are minimized with the use of a prism for dispersion. We present preliminary experiments on gold particles with 40 nm diameter are presented and show that the background suppression is large enough to measure the fluorescence of a single quantum dot in a scattering environment without the use of any filters.

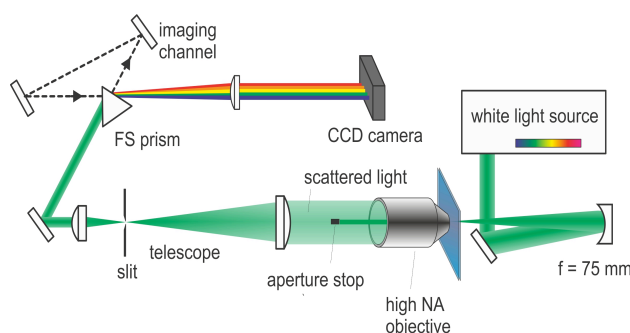


Figure 1: Setup of the dark-field microspectroscopy

## Experimental approach

The achievable brightness of the collected scattering signal and the spatial resolution depend critically on the numerical aperture with which scattered photons can be detected. In conventional dark-field microscopy, background photons are avoided by blocking the transmitted or reflected illumination beam after the objective, at the expense of inherently reducing the effective numerical aperture. A classic example is annular illumination, which cropping of a relatively large part of the detection cone. Here, we illuminated the sample instead with a 75 mm focusing mirror under normal incidence from the front and block the narrow collimated beam after the objective with a small aperture stop. The 10  $\mu\text{m}$  wide illumination spot is ideal for wide-field imaging of the sample. This allows us to measure the signals of a particle and its surroundings simultaneously.

The setup is illustrated in Fig. 1: The sample is illuminated with white light from a SuperK Extreme supercontinuum source (NKT Photonics), covering a spectral range from 430-800 nm. Transmitted and scattered light is collected with a 1.42 NA objective (Olympus PLAPON 60x). The aperture stop for blocking the illumination beam is only 1-2 mm in diameter, so that up to 95 % of the numerical aperture of the objective are used. The magnification is adjusted with a 3:1 telescope to optimize the imaging system for the relatively large pixel size of the CCD camera. A slit in the focal plane selects a single vertical slice of the 2-dimensional image, which is then dispersed with a fused silica prism and detected with a CCD camera (Rolera Thunder, QIMAGING). The use of a prism as the dispersing element reduces the losses to a minimum. The prism can be moved out of the beam path with a motorized translation stage (Agilis, Newport), opening an alternative imaging path (dashed black in Fig. 1). In this way the particle can be selected and precisely positioned with respect to the slit, ensuring reproducible detection with sub-nanometer spectral accuracy. Scattering cross section spectra were corrected by comparison with reference measurements of non-resonant scattering from latex beads.

## Sample Preparation

Streptavidin-functionalized gold particles (BBI solutions) and Latex bead samples (Sigma, 100 nm diameter) in aqueous solution were deposited onto the cover slip by spin coating. Streptavidin-functionalized quantum dots with an emission maximum at 655 nm (Invitrogen) were immobilized on a cover slip surface by binding to biotinylated bovine serum albumin bound non-specifically to the surface of the coverslip.

## Results and Discussion

Colloidal gold particles have been used for centuries for the staining of glass panes. Their color originates from a surface plasmon resonance around 530 nm and, in contrast to organic chromophores, they do not saturate upon illumination nor are subject to photobleaching. Together with their large scattering cross sections and stability this makes them ideal probes for a number of challenging applications in imaging and high-speed particle tracking.<sup>5,6</sup> We used single gold particles with an average diameter of 40 nm on a glass coverslip for a first experiment. Typical measured scattering spectra of individual particles are shown in Fig. 2, left. Although the size variation of the investigated particles is only around 8 %, large differences in the scattering cross-section were observed. Dark-field microscopy is highly sensitive to size variation, because the signal strength scales with the sixth power of the particle diameter, so even a 10% reduction in particle size decreases the amount of scattered power by half. We remark that the collected images and spectra represent the highest signal-to-noise ratio dark-field images ever obtained of nanoscopic particles

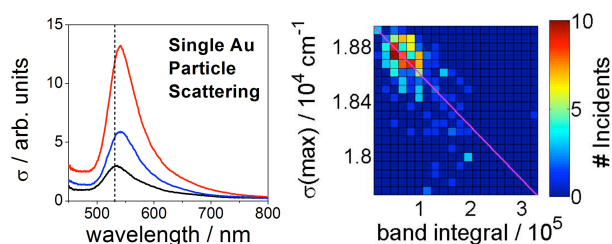


**Figure 2: Scattering spectra of single gold particles with 40 nm average diameter (left) and histogram over the band maximum  $\sigma(\max)$  and the band integral (right).**

The spectra in Fig. 2 also exhibit a red shift of the resonance band with increasing particle scattering cross section. The 2D histogram in Fig. 2 summarizes the spectral scattering properties of 190 single gold particles. The orientation of the distribution along a diagonal demonstrates the correlation between scattering intensity and resonance band position. This result agrees with Mie theory, which predicts a red shift of the resonance for larger particles due to retardation effects and higher-order multipole contributions.<sup>7</sup> Given the excellent images obtained for 40 nm particles, we believe that the detection limit will approach 10-20 nm particles, a several order of magnitude improvement in terms of scattered power of existing techniques.

The ultimate goal is to reach the sensitivity necessary to characterize luminescent particles in their dark state. One requirement is that fluorescence and scattering detection of a particle are synchronized, which is ideally achieved by measuring both on the same detector. For fluorescence measurements, the excitation light is commonly removed with a filter, but this is not necessary in spectrally resolved detection. As a model fluorophore we studied single quantum dots with an emission maximum around 655 nm, which were immobilized on a cover slip. As before, the sample was illuminated with white light, which was passed through a 600 nm short-pass filter. Fluorescence of the quantum dot can be seen as a bright line in the spectrally dispersed image in Fig. 3, top. Even without the use of filters, any background light is completely suppressed in the fluorescence region. At wavelengths below the excitation filter cut-off around 600 nm scattering signals are visible, mainly from non-fluorescent scatterers around the quantum dot. By forming the difference image between detection with the quantum dot in its 'on' and 'off' state, the pure quantum dot signal is isolated, see Fig. 3, bottom.

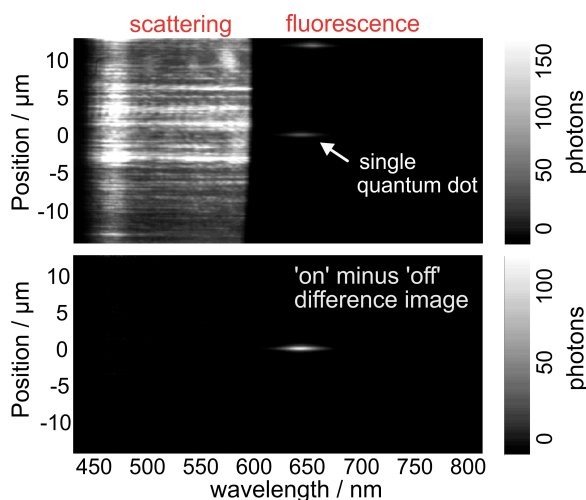


**Figure 3: Dispersed Images of a single quantum dot in a scattering surrounding: Raw image (top) and 'on' minus 'off' difference image of the blinking quantum dot (bottom).**

The semiconductor core of the measured quantum dots has a diameter of around 8 nm, and scattering of the quantum dot could not be identified at this stage. The strong size dependency of the scattering signal with the square of the volume renders the detection of small particles particularly demanding. However, when mixing the scattering field with a reference light field, the signal is only linearly dependent on the particle volume.<sup>8</sup> Based on this technique the first direct detection of scattering from a single quantum dot was reported in 2009.<sup>9</sup> It will be a future challenge to implement a similar approach into our spectrally resolved detection setup.

## Summary and Conclusions

We have developed a novel dark-field microscope for visible scattering spectroscopy of nanoparticles with unprecedented sensitivity. Front illumination with a curved mirror allows us to use an aperture stop to block the transmitted excitation light, so that 95 % of the numerical aperture are used for detection. Subsequent losses are minimized by the use of a prism for dispersion. Scattering spectra of single gold nanoparticles with an average diameter of 40 nm were measured. The variation in the total scattering cross section was correlated with the position of the resonance band, and was assigned to a distribution in the particle size. The efficient suppression of background light was demonstrated by the simultaneous measurement of the fluorescence of a single quantum dot and scattering from its surrounding. Scattering from the quantum dot itself still evades detection, but can become feasible by implementing a heterodyne detection scheme, in future.

## Acknowledgements

We are grateful to the Central Laser Facility for providing the SuperK Extreme supercontinuum source from their loan pool. A Weigel was supported by a Newton Fellowship of the Royal Society.

## References

1. J. Hohlbein, K. Gryte, M. Heilemann, A.N. Kapanidis, *Phys. Biol.* **2010**, *7*, 031001.
2. P. Kukura, M. Celebrano, A. Renn, V. Sandoghar, *J. Phys. Chem. Lett.* **2010**, *1*, 3323.
3. S. Chong, W. Min, X. Sunney Xie, *J. Phys. Chem. Lett.* **2010**, *1*, 3316.
4. A. Gaiduk, M. Yorulmaz, P.V. Ruijgrok, M. Orrit, *Science* **2010**, *330*, 353.
5. S. Eustis, M. A. El-Sayed, *Chem. Soc. Rev.* **2006**, *35*, 209.
6. J. Ortega-Arroyo, P. Kukura, *Phys. Chem. Chem. Phys.* **2012**, *14*, 15625.
7. S. Link, M.A. El-Sayed, *J. Phys. Chem. B* **1999**, *103*, 8410.
8. K. Lindfors, T. Kalkbrenner, P. Stoller, V. Sandoghdar, *Phys. Rev. Lett.* **2004**, *93*, 037401.
9. P. Kukura, M. Celebrano, A. Renn, V. Sandoghdar, *Nano Lett.* **2009**, *9*, 926.

# Confocal imaging of Z-combretastatin induced apoptosis and two-photon activation of E-combretastatin pro-drugs

Contact [kathrin.scherer@stfc.ac.uk](mailto:kathrin.scherer@stfc.ac.uk)

## K.M. Scherer

Central Laser Facility, STFC, Research Complex at Harwell, Didcot, OX11 0QX, UK

## R.H. Bisby

Biomedical Sciences Research Centre, University of Salford, Salford, M5 4WT, UK

## S.W. Botchway

Central Laser Facility, STFC, Research Complex at Harwell, Didcot, OX11 0QX, UK

## A.W. Parker

Central Laser Facility, STFC, Research Complex at Harwell, Didcot, OX11 0QX, UK

## Introduction

Combretastatins are highly potent vascular disrupting drug candidates used for the treatment of cancer [1] and potentially also wet age-related macular degeneration (AMD) [2]. A disodium phosphate salt of the natural product Combretastatin A-4 is currently entering phase III clinical trials for the treatment of advanced solid tumors [3]. The major drawback associated with the highly active Z-combretastatins (~ 1 nM on K562 cells) in clinical trials is their cytotoxicity towards healthy tissues leading to severe side effects such as cardio toxicity [4]. It is proposed that these side-effects are minimized by selectively localizing Z-combretastatin in cancerous tissues or abnormal vasculature only. This may be achieved by administering the E-combretastatin isomer as “inactive” pro-drug which can be converted to the active Z-isomers by selective irradiation using near-infrared (NIR) light (625 nm) two-photon (2P) excitation [5] [6]. NIR irradiation will be delivered by a fs-pulsed Ti:sapphire laser providing high peak powers and allows deep tissue penetration of the light [7].

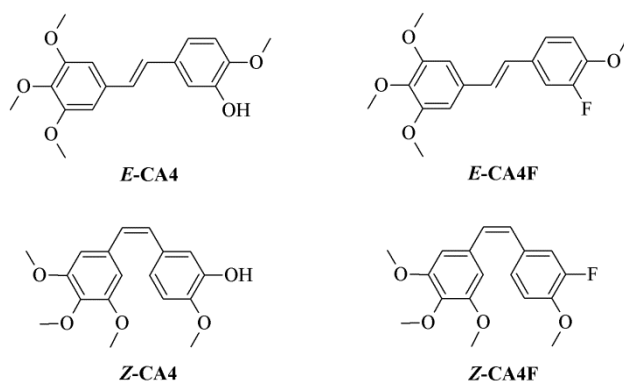


Figure 1: Structures of E- and Z-combretastatins studied

Here Z-combretastatin induced cell death (apoptosis) and 2P excited E-combretastatin activation on live cells leading to apoptotic activity were studied. The structures of the compounds of interest are shown in Figure 1.

## Materials & Methods

CHO (Chinese Hamster Ovary) and HeLa cells were obtained from the European Collection of Cell Cultures and maintained according to standard tissue culture procedures. HUVEC cells were purchased from TCS CellWorks and cultured following their guidelines [8]. For imaging, adherent cell cultures were grown in glass-bottom culture dishes (MatTek Corporation) and incubated at 37 °C, 5% CO<sub>2</sub>. The apoptosis markers propidium iodide and Annexin V AlexaFluor488 conjugate were purchased from Sigma Aldrich and Invitrogen respectively. Propidium iodide fluorescence was excited at 543 nm and Annexin V AlexaFluor488 fluorescence at 473 nm using the Nikon confocal microscope (20x objective) described in the

literature previously [9]. All images show overlays of a transmitted light image and the two confocal images obtained at each excitation wavelength.

## Z-combretastatin induced apoptosis on live mammalian cells

Cell killing (cytotoxic) effects of the Z-combretastatins Z-CA4 and Z-CA4F were investigated on CHO, HeLa and HUVEC cells. These three cell lines were chosen to show the activity of the Z-combretastatins towards normal (CHO), cancer (HeLa) and endothelial (HUVEC) cells. Endothelial cells such as HUVECs are the main target cells for combretastatins in living organisms since there are rapidly dividing within the tumor vasculature and shutdown of capillary vessels formed by these cells leads to tumor starvation.

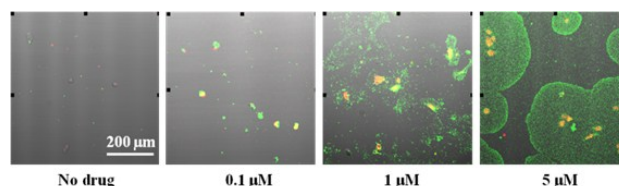


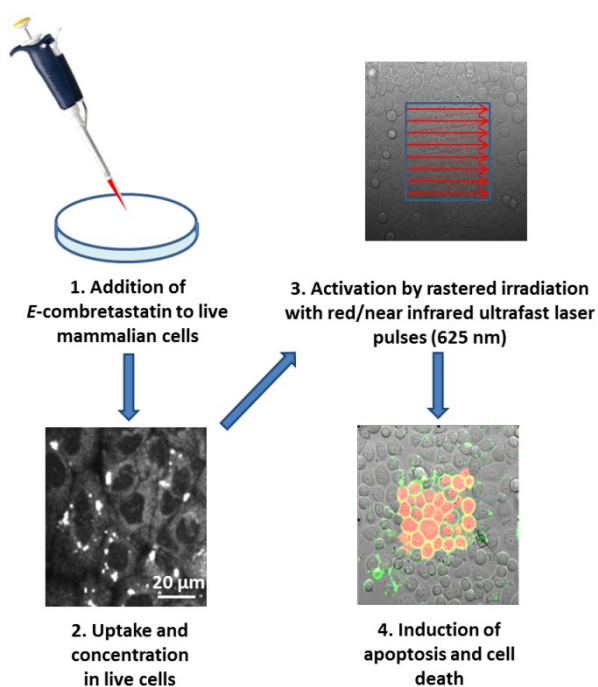
Figure 2: Apoptosis in HUVECs induced by incubation with increasing Z-CA4F concentrations for 24 h

Figure 2 shows a series of confocal images that were obtained 24 h after addition of increasing Z-CA4F concentrations (0, 0.1, 1 and 5 μM) to HUVEC cells at 37 °C. A small portion of the untreated control cells stained positive for the apoptosis markers, which is explained by a certain level of naturally occurring cell death in live cell cultures. This effect is even more prominent in primary cell lines such as HUVECs since they are known to be particularly sensitive to environmental changes compared with immortalized cell lines including CHO and HeLa cells. At the lowest Z-CA4F concentration (0.1 μM) a significant amount of cells displayed early apoptotic activity (Annexin V AlexaFluor488 conjugate binding) and a few cells stained positive for propidium iodide. At Z-CA4F concentrations ≥ 1 μM all cells stained positive for both apoptosis markers. Furthermore the HUVECs that were incubated at 5 μM presented spread out halos of membrane debris surrounding them. Summarizing both drugs, Z-CA4 and Z-CA4F, demonstrated significant activity towards all three cell lines with an increasing effect at higher drug concentrations and longer incubation times. The results confirm that HUVECs are more affected by treatment with the Z-combretastatins than CHO and HeLa cells as apoptosis marker binding was more prominent and halos of membrane debris were observed.

## E-combretastatin activation on live mammalian cells

After the use of propidium iodide and Annexin V AlexaFluor488 conjugate as markers for Z-combretastatin induced apoptosis on mammalian cells was shown to be a valid approach the next step was to demonstrate two-photon excited E-combretastatin pro-drug conversion to the active Z-isomer on

live cells. CHO cells were chosen for these experiments since they are the most stable of the cell lines used for this work. Monolayers of live CHO cells were incubated with the *E*-combretastatins, *E*-CA4 and *E*-CA4F, respectively for 2 h to allow uptake and accumulation of the pro-drug within the cells. Then a small area (100  $\mu\text{m}^2$ ) of the cell monolayer was raster-scanned with the pulsed beam output from a Ti-sapphire laser (625 nm) for 10 min converting the *E*-combretastatin to its highly active *Z*-isomer. After 24 h the markers for apoptosis (propidium iodide and Annexin V AlexaFluor488 conjugate) were added and selective cell killing (cytotoxicity) within the irradiated areas was observed using confocal microscopy (Figure 3).



**Figure 3:** Two-photon activation of *E*-combretastatins on monolayers of live CHO cells and cell killing. **1.** The *E*-combretastatin was added to confluent live CHO cells at a concentration of 25  $\mu\text{M}$  and **2.** incubated for 30 min. **3.** A pulsed laser beam (625 nm) was raster-scanned over an area of 100  $\mu\text{m}^2$  for 10 min (4.5 mW laser power). **4.** Staining with propidium iodide and Annexin V AlexaFluor488 conjugate showed cell killing by the activated pro-drug within 24 h.

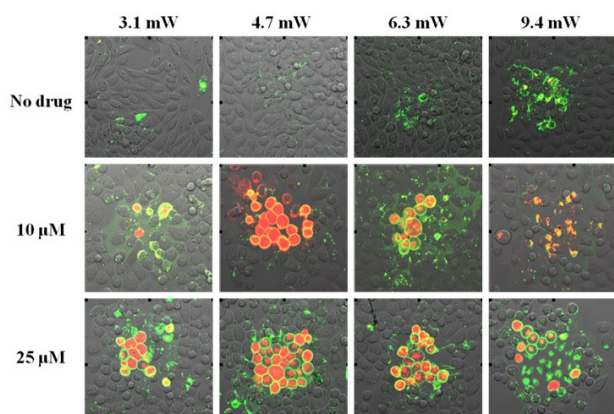


**Figure 4:** CHO cells incubated with *E*-CA4F (0, 10, and 25  $\mu\text{M}$ ) for 2 h before irradiation of a 100  $\mu\text{m}^2$  field for 10 min at 625 nm and increasing laser powers at the sample (3.1, 4.7, 6.3 and 9.4 mW). 24 h after irradiation CHO cells were stained with Annexin V AlexaFluor488 conjugate and propidium iodide to determine the extent of apoptosis.

Figure 4 shows a set of results for the pro-drug activation experiment using *E*-CA4F as pro-drug candidate at different concentrations (0, 10 and 25  $\mu\text{M}$ ) and activated at different laser powers (3.1, 4.7, 6.3 and 9.4 mW). For both pro-drug

candidates, *E*-CA4 and *E*-CA4F, only partial conversion of the pro-drug to the active *Z*-isomer was observed by confocal imaging of propidium iodide and Annexin V staining at the lowest laser power (3.1 mW). The best results at all three pro-drug concentrations (10, 25 and 50  $\mu\text{M}$ ) were obtained when exciting with a laser power of 4.7 mW at 625 nm. At the two high powers (6.4 and 9.4 mW) cell damage induced by the laser light alone was observed. At the highest concentration (50  $\mu\text{M}$ ) *E*-CA4F started to precipitate from solution, so the actual concentration on the cells was not known and it is hence recommended to use lower *E*-CA4F concentrations to obtain reliable results. This effect was not seen with *E*-CA4, which has slightly better water-solubility. It was observed that 24 h after drug activation apoptosis only occurred within the irradiated areas, whereas surrounding cells were still alive.

## Conclusions

In summary the experiments demonstrated that *Z*-combretastatins (*Z*-CA4 and *Z*-CA4F) induce apoptosis on a range of mammalian cell lines at a rate that increases with drug concentration and incubation time. The level of apoptosis also varied depending on the cell type used, being higher for the very sensitive primary HUVECs compared with CHO and HeLa cells. Pro-drug photoactivation experiments using *E*-CA4 and *E*-CA4F on monolayers of CHO cells showed that the pro-drug candidates are activated highly selectively by two-photon excitation at 625 nm. The irradiation power needs to be chosen carefully to achieve sufficient *E*→*Z* conversion. At the same time it is important that the laser power is low enough to not cause cell damage by irradiation alone. The apoptosis staining procedure devised herein was shown to allow visualization of the induction of apoptosis by *Z*-combretastatins by distinguishing between live and apoptotic cells. A disadvantage of this method is that reliable quantification is challenging. Based on the initial success demonstrating cell killing after 2P excited pro-drug activation on monolayers of live cells it is suggested that future experiments should investigate the photoactivation of *E*-combretastatins within three dimensional (3D) tissue models, such as cell scaffold models (e.g. electrospun or Alvetex), hydrogels and spheroids, to mimic real tissues more closely. It is hoped that 2P *E*-combretastatin activation may be demonstrated at depths > 1 mm in tissue models or even within live tissues.

## Acknowledgements

We thank Alan McGown and John Hadfield at the University of Salford for their help with the synthesis of target compounds and discussions. We acknowledge the STFC Biomed network and the University of Salford for providing a studentship to KMS and the STFC Futures programme for providing funding to carry on this work.

## References

1. Griggs, J. *et al.* (2001). *Lancet Oncol.*, **2**, 82-87.
2. Ibrahim, M.A. *et al.* (2013). *BMC Pharmacol. & Toxicol.*, **14**, 1-10.
3. ClinicalTrials.gov (2012). Retrieved July 10, 2013 from <http://clinicaltrials.gov/ct2/show/NCT01701349?term=combretastatin&rank=14>.
4. Rustin, G.J. *et al.* (2010). *Br. J. Cancer*, **102**, 1355-1360.
5. Bisby, R.H. *et al.* (2012). *Eur. J. Cancer*, **48**, 1896-1903.
6. Bisby, R.H. *et al.* (2012). *Meas. Sci. Technol.*, **23**, 1-10.
7. Helmchen F. & Denk, W. (2005). *Nature Methods*, **2**, 932-940.
8. TCS CellWorks (2009). *The Culture of Primary Human Cells – An Instruction Manual*, 1-13.
9. Botchway, S.W. *et al.* (2012). *Meth. Enzymol.*, **504**, 3-28.